The Geological Society of America
Special Paper 438
2008

# *Geochemistry and geology of the Iron Mountain unit, Ingalls ophiolite complex, Washington: Evidence for the polygenetic nature of the Ingalls complex*

**J.H. MacDonald Jr.**[†]
**G.D. Harper**
*Department of Earth and Atmospheric Sciences, University at Albany, New York 12222-0001, USA*

**R.B. Miller**
**J.S. Miller**
**A.N. Mlinarevic**
*Department of Geology, San Jose State University, San Jose, California 95192-0102, USA*

**B.V. Miller**
*Department of Geology & Geophysics, Texas A&M University, College Station, Texas 77843-3115, USA*

## ABSTRACT

**The Ingalls ophiolite complex, central Cascades, Washington, mainly consists of mantle-derived ultramafic tectonite, with crustal rocks consisting of gabbro, diabase, basalt, and sedimentary rocks. The crustal rocks occur as faulted blocks within serpentinite mélange (Navaho Divide fault zone). Mafic rocks in most of these blocks comprise the Late Jurassic Esmeralda Peaks unit. Herein, we define an older, Early Jurassic unit within the Ingalls ophiolite complex, which we call the Iron Mountain unit. This unit occurs along the southern edge of the complex and consists dominantly of mafic volcanic rocks with minor sedimentary rocks. A rhyolite within the Iron Mountain unit yields a ca. 192 Ma U-Pb zircon age, consistent with an Early Jurassic age assignment based on radiolarians in cherts. The presence of volcanic rocks that have within-plate basalt magmatic affinities and oolitic limestone suggests that the Iron Mountain unit formed as a seamount. Magmatic affinities range from within-plate basalt to enriched mid-ocean-ridge basalt (E-MORB), which is compatible with a mantle plume close to a ridge. The Early Jurassic age of the Iron Mountain unit, which is ~30 m.y. older than the Esmeralda Peaks unit, indicates that the Ingalls ophiolite complex is polygenetic. The Iron Mountain unit most likely represents basement that was rifted in a suprasubduction-zone setting in the Late Jurassic during formation of the Esmeralda Peaks unit.**

**Keywords:** Ingalls, seamount, Jurassic, polygenetic, ophiolite.

[†]Department of Marine and Ecological Sciences, Florida Gulf Coast University, 10501 FGCU Boulevard, South, Fort Myers, Florida 33965, USA; e-mail: jmacdona@fgcu.edu.

MacDonald, J.H., Jr., Harper, G.D., Miller, R.B., Miller, J.S., Mlinarevic, A.N., and Miller, B.V., 2008, Geochemistry and geology of the Iron Mountain unit, Ingalls ophiolite complex, Washington: Evidence for the polygenetic nature of the Ingalls complex, *in* Wright, J.E., and Shervais, J.W., eds., Ophiolites, Arcs, and Batholiths: A Tribute to Cliff Hopson: Geological Society of America Special Paper 438, p. 161–173, doi: 10.1130/2008.2438(05). 

## INTRODUCTION

Ophiolites are generally considered to be fragments of oceanic crust and upper mantle that formed during seafloor spreading and that have been emplaced onto continents (e.g., Anonymous, 1972; Moores, 1982; Dilek, 2003). Some terranes referred to as ophiolitic have older basement rocks and have been interpreted as rift-edge facies (De Wit and Stern, 1981; Saleeby et al., 1982; Wyld and Wright, 1988; Dewey, 2003; Stern and De Wit, 2003). A rift-edge facies represents volcanic and/or intrusive rocks that form prior to opening of a basin by seafloor spreading, and thus they lie along the margins of a basin. These rocks are built on, or intruded into, basement that predates spreading. Still other incomplete "ophiolites" are interpreted to have formed as seamounts rather than by seafloor spreading or rifting (MacPherson, 1983; Meyer et al., 1996; Eddy et al., 1998; Dewey, 2003; Shervais et al., 2005).

A belt of Middle to Late Jurassic ophiolites extends along the western coast of North America for over 1000 km (Fig. 1). Understanding of the origin of this ophiolite belt is fundamental to understanding the Jurassic tectonic history of the western North America Cordillera (Saleeby, 1992). Included within this belt are the Josephine ophiolite and its rift-edge facies, which were built upon the older ophiolitic Rattlesnake Creek terrane, the Kings-Kaweah belt, the Coast Range ophiolite, and the Ingalls ophiolite complex (Fig. 1) (Saleeby, 1978; Saleeby and Sharp, 1980; Hopson et al., 1981; Saleeby et al., 1982; Miller, 1985; Wyld and Wright, 1988; Miller et al., 1993; Harper et al., 1994, 2003; Shervais et al., 2004).

The Ingalls ophiolite complex is the largest and most complete of the northern ophiolites of this belt, and it has been correlated with the ca. 162 Ma Josephine ophiolite (Fig. 1) (Miller et al., 1993; Metzger et al., 2002; Miller et al., 2003). It is intruded by the 91–96.5 Ma Mount Stuart batholith, overlain by Eocene sediments to the south, and thrust over the Chiwaukum Schist along the Cretaceous Windy Pass thrust to the north (Fig. 2) (Miller, 1980, 1985; Matzel et al., 2006).

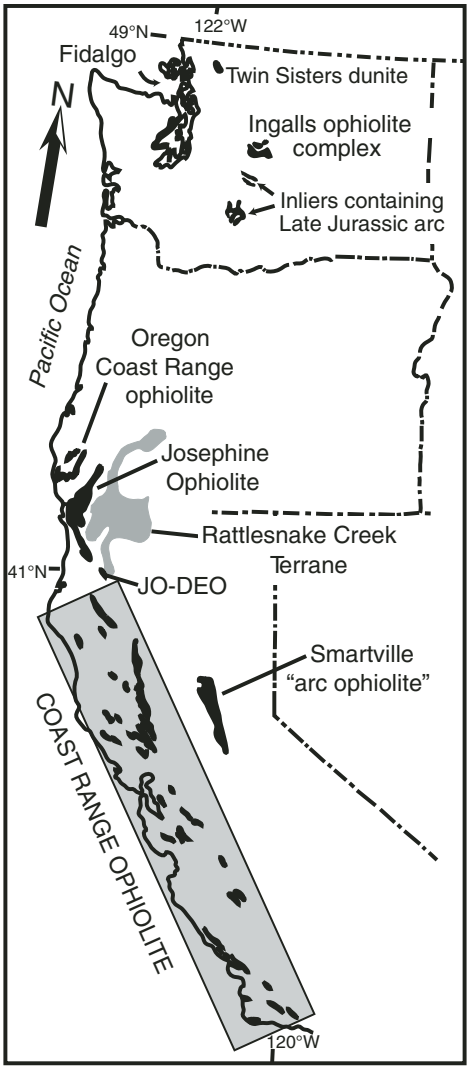


Figure 1. Location of Middle to Late Jurassic ophiolites of the North America Cordillera and older Rattlesnake Creek terrane. JO-DEO—Devils Elbow. Figure was modified from Metzger et al. (2002).

## INGALLS OPHIOLITE COMPLEX

The Ingalls ophiolite complex principally consists of mantle peridotite. Subordinate crustal rocks, as well as peridotite, occur as outcrop- to kilometer-scale, fault-bounded blocks that are encased within the serpentinite mélange of the Navaho Divide fault zone. These include the Ingalls sedimentary rocks (Peshastin Formation) and mafic rocks of the Esmeralda Peaks and Iron Mountain units.

### Mantle Peridotites

The relationship between the voluminous peridotite tectonites (Fig. 2) and crustal units of the Ingalls ophiolite complex is not well understood. A northern lherzolite and clinopyroxene-rich harzburgite unit is separated from a southern harzburgite and dunite unit by the Navaho Divide fault zone (Fig. 2) (Miller, 1985). The Navaho Divide fault zone (Figs. 2 and 3) is a mélange that consists of sheared serpentinite matrix that encases fault-bounded blocks of less serpentinized peridotite and the crustal units (Miller, 1980, 1985; Miller and Mogk, 1987). The faulted contacts of mélange blocks dip steeply to the north (Miller, 1980, 1985). The shear fabric of the Navaho Divide fault zone mélange overprints mylonitic lherzolite that is transitional into the northern lherzolite unit (Fig. 2) (Miller, 1985; Miller and Mogk, 1987). Miller (1985) and Miller and Mogk (1987) proposed that the Navaho Divide fault zone originated as a transform fault and fracture zone.

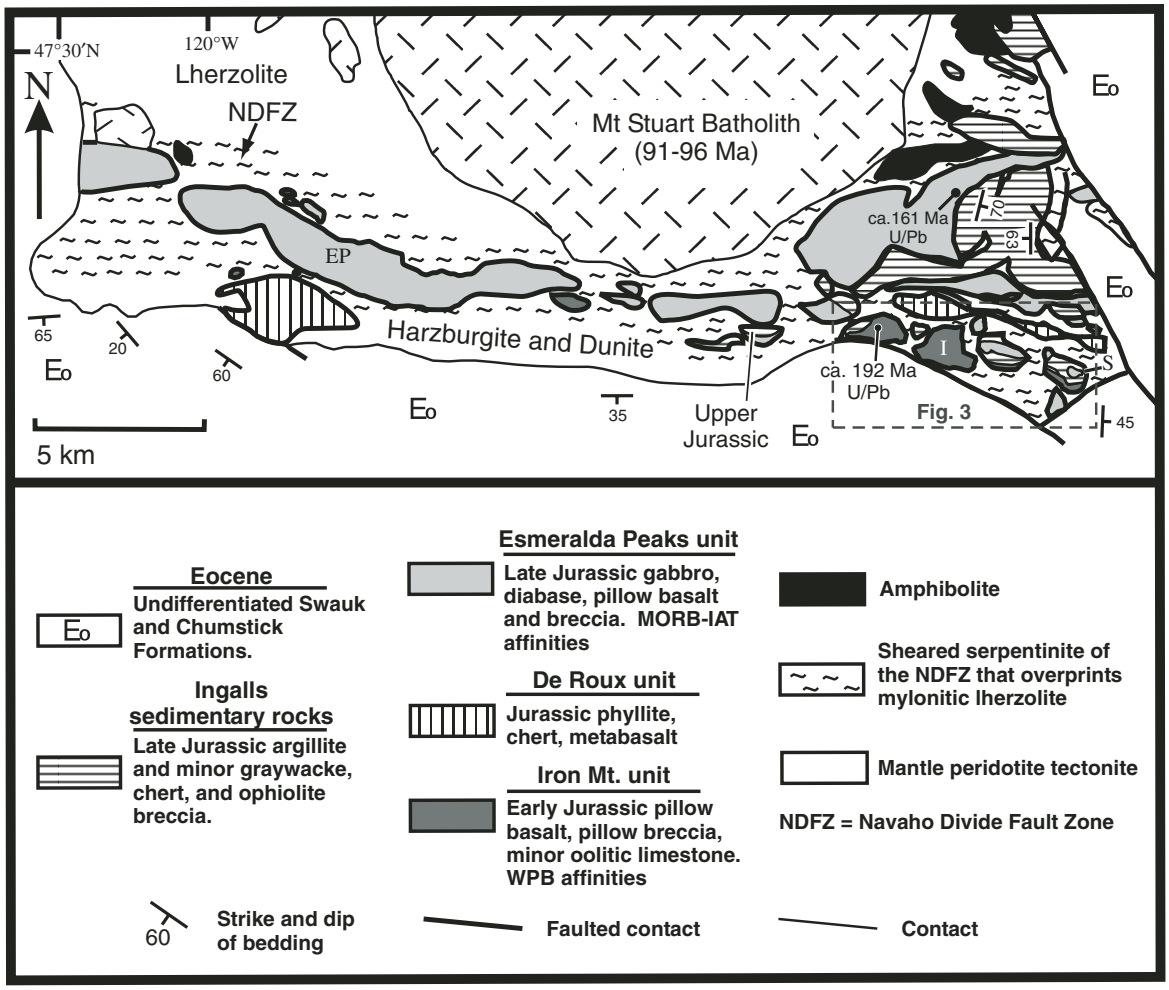


Figure 2. Geologic map of the Ingalls ophiolite complex and surrounding units. EP—Esmeralda Peaks; NDFZ—Navaho Divide fault zone; I—Iron Mountain; S—Sheep Mountain. IAT—island-arc tholeiite; MORB—mid-ocean-ridge basalt; WPB—within-plate basalt. Indicated Jurassic ages are based on radiolariain chert (E. Pessagno, 2002, personal commun. to MacDonald et al., this volume, chapter 4).

## Esmeralda Peaks Unit

The Esmeralda Peaks unit consists of gabbro, sparse plagiogranite, abundant diabase (locally forming sheeted dikes), pillowed and massive basalt, and minor ophiolitic breccia and intrapillow chert (Miller, 1985; Harper et al., 2003; MacDonald et al., this volume, chapter 4). A gabbro from this unit has yielded a U-Pb zircon age of 161 ± 1 Ma (2σ) (Fig. 2) (Miller et al., 2003). Geochemical affinities of Esmeralda Peaks volcanic rocks are transitional from mid-ocean-ridge basalt to island-arc tholeiite (MORB-IAT), although a few lava samples have boninitic affinities (Metzger et al., 2002; Harper et al., 2003; MacDonald et al., this volume, chapter 4). This unit is interpreted to have formed in a back-arc basin cut by a fracture zone (Miller et al., 1993; Metzger et al., 2002; Harper et al., 2003; MacDonald et al., this volume, chapter 4). For a detailed discussion of the Esmeralda Peaks unit, refer to MacDonald et al. (this volume, chapter 4).

## Ingalls Sedimentary Rocks

The Ingalls sedimentary rocks occur primarily in the eastern portion of the complex (Figs. 2 and 3) (Smith, 1904; Southwick, 1962, 1974; Tabor et al., 1982; Mlinarevic et al., 2003). Argillite predominates, and chert, graywacke, conglomerate, ophiolitic breccia, and sedimentary serpentinite are minor constituents (Fig. 4) (Smith, 1904; Southwick, 1962, 1974; Mlinarevic et al., 2003; MacDonald et al., 2005). These sedimentary rocks depositionally overlie the volcanic and plutonic rocks of the Esmeralda Peaks unit. Oxfordian and Kimmeridgian radiolaria occur

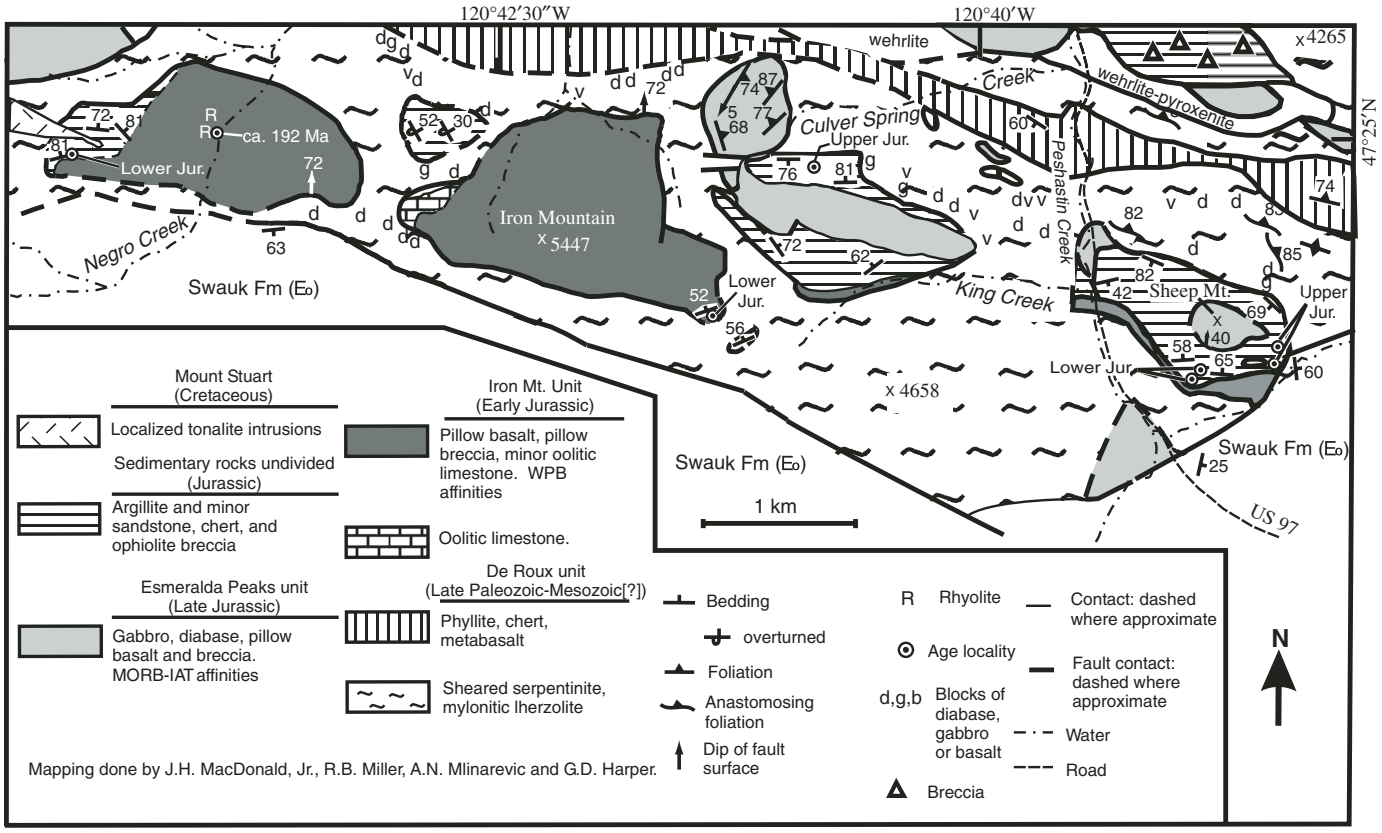


Figure 3. Geologic map of the southeastern part of the Ingalls ophiolite complex. Jurassic ages are based on radiolaria (Miller et al., 1993; C. Blome, 1992, personal commun.; E. Pessagno, 2002, 2004, personal commun.). Figure was modified from Tabor et al. (1982, 1987, 1993, 2000) and Harper et al. (2003). WPB—within-plate basalt.

within cherts from the Ingalls sedimentary rocks (Figs. 2, 3, and 4) (Miller et al., 1993; Pessagno, 2002, personal commun.; Harper et al., 2003). Ion microprobe U-Pb dating of detrital zircons from an Ingalls graywacke gives a bimodal age distribution, and the younger 153 Ma detrital zircon peak is interpreted to be the approximate age of deposition (Miller et al., 2003). Both a local ophiolite source and a distal terrigenous source are inferred for the Ingalls sedimentary rocks (Mlinarevic et al., 2003).

## Iron Mountain Unit

The Iron Mountain unit (Figs. 2 and 3), described in detail here for the first time, consists of volcanic and minor sedimentary rocks (Fig. 4). This unit occurs as kilometer-scale, and smaller, fault blocks within the serpentinite mélange of the steeply north-dipping Navaho Divide fault zone (Figs. 2 and 3). Faulted blocks of the Iron Mountain unit range in thickness from ~100 to >930 m (Fig. 4) and extend discontinuously for ~24 km in the southern part of the complex (Figs. 2 and 3). The Iron Mountain unit differs from the Esmeralda Peaks unit by its lack of gabbro and diabase, more abundant and well-developed pillows, and interlayered oolitic limestone (see following discussion).

### *Lithologies*

Volcanic rocks in the Iron Mountain unit include basalt flows and broken pillow breccia, and minor hyaloclastite and rhyolite. Most basalt is vesicular and pillowed; pillows range from ~10 cm to ~1 m in diameter. Sparse massive vesicular and sheet flows are intercalated with the pillow basalts and range up to ~2 m in thickness.

Plagioclase microglomerophenocrysts set in an altered glassy groundmass with plagioclase microlites are common in the basalts. Clinopyroxene was observed in the groundmass in several samples, and as microphenocrysts in one sample. The broken pillow breccia is monolithologic, consists of decimeter-size, angular, typically vesicular, fragments of pillows set in a matrix of altered glass, recrystallized calcite, and minor chert, and it makes up roughly one-third of all volcanic rocks. This broken pillow breccia occurs as both meter-scale outcrops interfingered with the pillow basalts, and as bodies extending laterally for up to ~685 m and reaching ~52 m in thickness. The hyaloclastite consists of altered mafic glass and <10% pillow basalt fragments. These hyaloclastites are commonly medium-bedded, are no more than a few meters in thickness, and make up <1% of all volcanic rocks. The rhyolite has quartz and plagioclase phenocrysts or, more frequently, microphenocrysts set

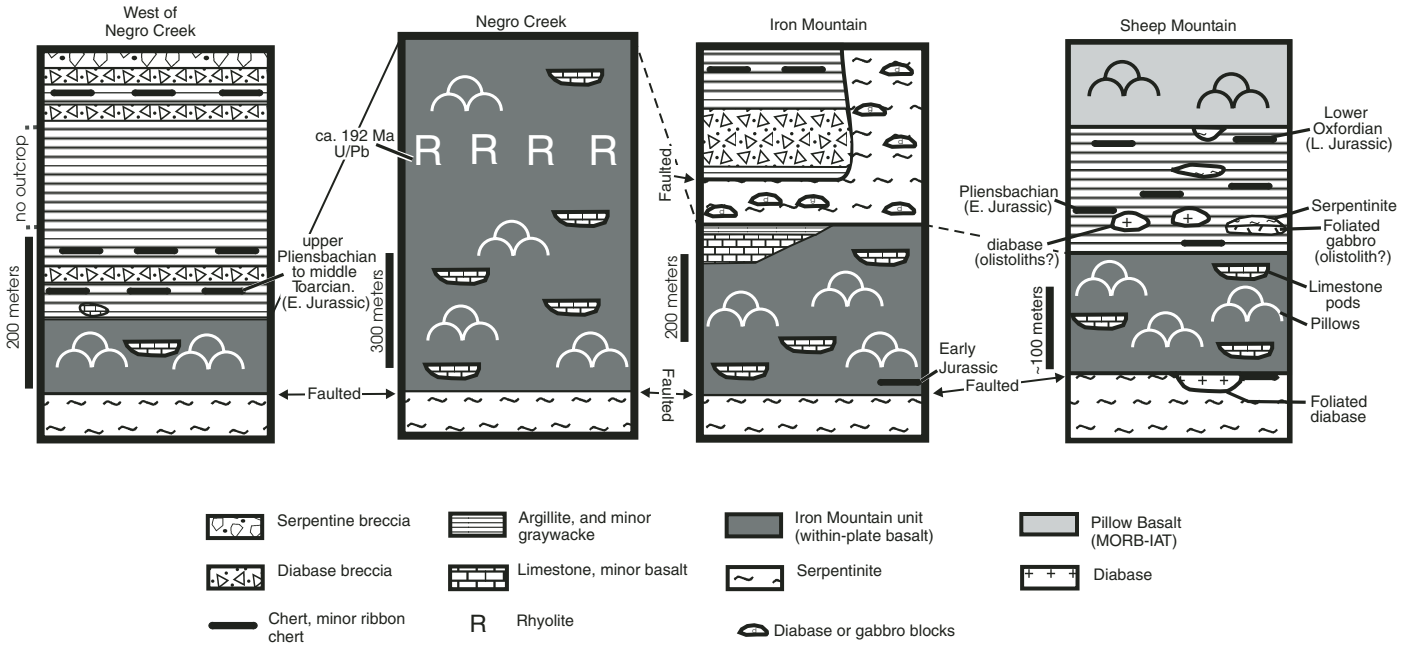


Figure 4. Stratigraphic section (synthesized from map; not measured) of Sheep Mountain, Iron Mountain, Negro Creek, and west of Negro Creek. Radiolarian ages are from Miller et al. (1993), C. Blome (1992, written commun.), and E. Pessagno (1999, written commun.).

in a granular groundmass of plagioclase and quartz. Sulfide mineralization occurs in the rhyolite. At one locality, rhyolite occurs as massive flows above broken pillow breccia and below vesicular pillow basalt and is up to ~65 m thick (Figs. 3 and 4).

Basalt flows and broken-pillow breccias have albite, epidote, chlorite, pumpellyite, and sphene as alteration minerals. Vesicles in the basalts are filled with calcite generally intergrown with epidote and pumpellyite. The rhyolite has albite, epidote, recrystallized quartz, and minor chlorite and sphene as alteration minerals. Secondary muscovite occurs in the rhyolite groundmass in one sample. Veins of calcite, and calcite plus quartz, cut the basalt and rhyolite, respectively. These mineral assemblages are consistent with greenschist-facies metamorphism.

Limestone and minor argillite, chert, and basaltic tuff are found intercalated with the volcanic rocks (Fig. 4). Pink and gray recrystallized limestone occurs as interpillow sediment up to ~1 m in diameter and, in places, is uniformly distributed throughout the pillow basalts. Interpillow argillites are locally siliceous, and impure chert occurs as recrystallized dark-green intrapillow sediments.

Basaltic tuffs occur between pillows as undisrupted aqueous deposits and as reworked beds. The reworked basaltic tuffs form ~1-cm-thick beds, with total bedded thickness ranging up to several meters (Miller, 1980). These reworked tuffs are monolithologic, consisting of poorly sorted millimeter- to centimeter-size basaltic fragments (Miller, 1980).

Mudstone, limestone, chert, basaltic breccia, and minor sandstone sit conformably on the volcanic rocks of the Iron Mountain unit. Mudstone is the most abundant sedimentary rock type. Locally interbedded with the mudstone is dark gray, thin- to medium-bedded radiolarian chert, jasper, red radiolarian chert, and ribbon chert (Figs. 3 and 4) (Harper et al., 2003). Radiolarian chert layers range from a few centimeters to a few meters in thickness. Basalt breccia consists of decimeter-size fragments cemented by recrystallized calcite, is up to ~21 m thick, and is moderately sorted. Thin beds of graywacke are massive to well bedded (millimeter- to centimeter-scale), poorly to weakly graded, and poorly sorted. Clasts of tuff and chert are common. These sandstones are more clay rich and more poorly sorted than Late Jurassic sandstones that overlie the Esmeralda Peaks unit (Southwick, 1962; MacDonald et al., this volume, chapter 4).

Limestone is a minor but distinctive rock type of the Iron Mountain unit (Figs. 3 and 4). It occurs as beds up to 80 m thick that lie conformably on the basalt (Fig. 4). The limestones are massive and are either light-gray or reddish-pink. Locally, the limestone is brecciated, with clasts up to 8 cm in diameter. The gray limestone is oolitic (Fig. 5) and contains fragments of echinoderms, foraminifera, bivalves, and possibly gastropods, as well as red and green algae (C.H. Stevens, 2002, personal commun.). The fossil fragments are commonly encased in the center of the ooids by microcrystalline calcite, and some ooids are composite. The red limestone is micritic, contains radiolarians and foraminifera, and is pelagic in origin (E. Pessagno, 2004, personal commun.).

### *Geochemistry*

Iron Mountain unit basalts were previously analyzed by Gray ($n = 6$; 1982) and Metzger et al. ($n = 2$; 2002). No localities were given for Gray's (1982) samples, which were interpreted

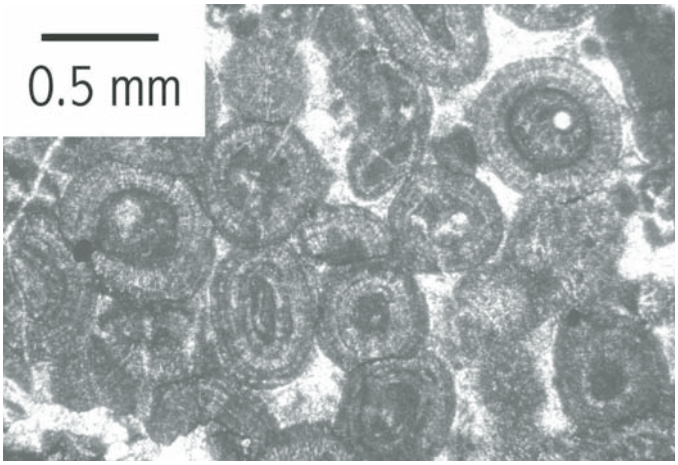


Figure 5. Photomicrograph of oolites in limestone within the Iron Mountain unit.

to have mid-ocean-ridge basalt (MORB) affinities. Metzger et al. (2002) recognized within-plate basalt affinities for their samples and similarly reinterpreted Gray's (1982) samples. Metzger et al. (2002) also suspected that the within-plate basalt samples belonged to a previously unrecognized unit within the Ingalls ophiolite complex.

Ten new Iron Mountain samples were analyzed for this paper (Table 1; see GSA Data Repository[1] for analytical discussion). In our evaluation of the Iron Mountain unit, we utilized the samples of Metzger et al. (2002) but excluded those of Gray (1982) due to the lack of published sample localities. Because the volcanics of the Iron Mountain unit underwent greenschist-facies metamorphism, only geochemical plots with elements that are immobile under these metamorphic conditions are used.

With the exception of two samples, basalts of the Iron Mountain unit have within-plate basalt affinities as evident from the Ti-Zr-Y diagram (Fig. 6; Table 1). According to Pearce (1996a), this diagram is extremely diagnostic for discriminating basalts that formed in a within-plate environment, probably because Y is depleted during partial melting of garnet lherzolite. The Th/Yb-Ta/Yb diagram (Fig. 7) indicates that the Iron Mountain basalts have within-plate enrichment of the mantle source, are transitional between tholeiitic and alkaline, and display no arc component. Ti/V ratios for the Iron Mountain unit basalts are transitional between alkaline and tholeiitic and are similar to those of Hawaii (Fig. 8). These basalts have steep negative slopes on MORB- and chondrite-normalized diagrams, and they display strong large ion lithophile element enrichment when compared to normal (N) MORB (Fig. 9; Metzger et al., 2002).

A rhyolite from the Iron Mountain unit also has within-plate affinities and has no arc component (Figs. 7 and 9; Table 1). The Th/Yb-Ta/Yb and rare earth element (REE) patterns are similar to the basalts from this unit (Figs. 7 and 9), except that the rhyolite displays a large negative Ti anomaly and a negative Eu anomaly (Fig. 8B), which are consistent with Fe-Ti oxide and plagioclase fractionation, respectively.

The two westernmost exposures of the Iron Mountain unit, located south of Esmeralda Peaks (Fig. 2), occur as isolated blocks within serpentinite-matrix mélange. These exposures have well-developed vesicular pillow basalt with abundant interpillow limestone, minor interpillow chert and basalt breccia, and rare argillite. Unlike similar rocks to the east, a sample from each locality has enriched mid-ocean-ridge basalt (E-MORB), rather than within-plate basalt, chemical affinities (Figs. 7 and 9). Like other Iron Mountain basalts, these two samples display no arc component (Fig. 7) but were derived from a mantle more depleted than other samples (Figs. 7 and 9).

### *Geochronology*

A U-Pb zircon date (Table 2; Fig. 10) of five handpicked, euhedral zircons has been obtained from a rhyolite west of Negro Creek (Figs. 3 and 4). Analysis was performed with a Micromass Sector 54 thermal ionization mass spectrometer at the University of North Carolina. Decay constants used were $^{238}U = 0.155125 \times 10^{-9}$ yr$^{-1}$, and $^{235}U = 0.98485 \times 10^{-9}$ yr$^{-1}$ (Steiger and Jäger, 1977). Weights were estimated using a video camera and are known to within 10%. Data reduction and error analysis was done using PbMacDat-2 by D.S. Coleman, using the algorithms of Ludwig (1989, 1990). All zircons were extensively air abraded and do not show any appreciable inheritance. The two most concordant zircons have ages of 192 Ma and are less than 0.7% discordant (Table 2). A weighted mean concordia age for all five zircons of 192.1 ± 0.3 Ma (means square of weighted deviates [MSWD] of concordance = 3.3, including 2σ decay constant errors; Fig. 10) is taken as the preferred age.

Pliensbachian and Upper Pliensbachian to Middle Toarcian radiolarians (*Paracanoptum annulatum* and *Parahsuum* sp.; zone 01, base subzone 1A to top of subzone 01B; Pessagno and Poisson, 1979) are reported from cherts within the Iron Mountain unit (Figs. 3 and 4; Table 3) (C. Blome, 1992, written commun.; E. Pessagno, 2004, written commun.). The Lower Jurassic radiolarian chert occurs at three localities: (1) interbedded with Iron Mountain unit pillow basalt ~1.8 km east of the summit of Iron Mountain, on the drainage divide south of King Creek (probable late Pliensbachian age; Table 3; Figs. 3 and 4); (2) interbedded with argillite ~50 m above Iron Mountain basalt on Sheep Mountain (Pliensbachian age; Table 3; Figs. 3 and 4); and (3) interbedded with argillite ~35 m above Iron Mountain basalt west of Negro Creek (Upper Pliensbachian to Middle Toarcian; Table 3; Figs. 3 and 4). This Pliensbachian to probable late Pliensbachian age is slightly younger than the ca. 192 Ma zircon age (Fig. 10) based on the Gradstein et al. (2004) Jurassic time scale (Pliensbachian = 189 ± 1.5–183 ± 1.5 Ma) (Tables 2 and 3; Figs. 3, 4, and 10). The time scale of Palfy et al. (2000), however, places the Pliensbachian at 196.5 Ma (+1.7/–5.7) and 191.5 Ma (+1.9/–4.7).

[1]GSA Data Repository Item 2008065, Analytical methods, is available on request from Documents Secretary, GSA, P.O. Box 9140, Boulder, CO 80301-9140, USA, or editing@geosociety.org, at www.geosociety.org/pubs/ft2008.htm.

TABLE 1. ANALYSES OF IRON MOUNTAIN UNIT BASALT AND RHYOLITE SAMPLES

| Sample: | BL-14–1[§§] | BL-95–1 | BL-150 | DRJM-16A | EL-42–2[§§] | IM-01A | IM-17 | IM-32 | IM-4 | IM-40A | IM-70 | IOE-77H |
|---|---|---|---|---|---|---|---|---|---|---|---|---|
| Rock type: | pillow basalt | pillow basalt | rhyolite | pillow basalt | pillow basalt | pillow basalt | pillow basalt | pillow basalt | pillow breccia | pillow basalt | pillow basalt | pillow basalt |
| Latitude:[†] | N47 24.126 | N47 24.786 | N47 25.090 | N47 25.966 | N47 25.631 | N47 24.631 | N47 24.711 | N47 24.760 | N47 24.910 | N47 24.454 | N47 24.949 | N47 25.776 |
| Longitude: | W120 38.677 | W120 41.550 | W120 44.005 | W120 59.151 | W120 51.401 | W120 42.644 | W120 42.812 | W120 42.812 | W120 43.444 | W120 41.426 | W120 44.665 | W120 57.756 |
| Magma type:[‡] | WPB | WPB | WPG | E-MORB | WPB | WPB | WPB | WPB | WPB | WPB | WPB | E-MORB |
| $SiO_2$ | 41.20 | 47.59 | 74.76 | 49.32 | 49.69 | 47.37 | 50.60 | 49.77 | 51.51 | 51.81 | 51.43 | 50.49 |
| $Al_2O_3$ | 14.16 | 16.43 | 13.17 | 17.36 | 14.33 | 18.30 | 13.97 | 16.24 | 16.28 | 14.83 | 13.70 | 17.57 |
| $TiO_2$ | 4.20 | 1.96 | 0.19 | 1.88 | 2.62 | 1.94 | 3.33 | 3.43 | 1.84 | 3.26 | 2.88 | 1.29 |
| $FeO^{T}$[§] | 11.05 | 8.84 | 2.94 | 11.50 | 12.15 | 12.21 | 13.00 | 11.53 | 9.69 | 11.68 | 13.59 | 11.18 |
| MnO | 0.20 | 0.17 | 0.03 | 0.17 | 0.20 | 0.14 | 0.18 | 0.12 | 0.15 | 0.12 | 0.21 | 0.19 |
| MgO | 2.91 | 6.42 | 0.12 | 2.48 | 4.37 | 3.29 | 3.94 | 2.13 | 6.61 | 3.53 | 5.78 | 6.86 |
| CaO | 21.69 | 14.49 | 0.71 | 9.74 | 9.90 | 12.41 | 10.23 | 10.28 | 8.64 | 8.55 | 7.27 | 6.98 |
| $Na_2O$ | 2.85 | 3.65 | 4.86 | 4.20 | 5.74 | 3.91 | 4.10 | 4.68 | 4.78 | 4.80 | 4.44 | 4.71 |
| $K_2O$ | 1.03 | 0.10 | 3.19 | 3.00 | 0.66 | 0.14 | 0.27 | 1.29 | 0.27 | 0.98 | 0.37 | 0.58 |
| $P_2O_5$ | 0.72 | 0.35 | 0.04 | 0.36 | 0.34 | 0.30 | 0.38 | 0.53 | 0.23 | 0.43 | 0.33 | 0.14 |
| Total[#] | 100.00 | 100.00 | 100.00 | 100.00 | 100.00 | 100.00 | 100.00 | 100.00 | 100.00 | 100.00 | 100.00 | 100.00 |
| LOI | N.D.[‡‡] | 7.33 | 1.14 | 5.62 | N.D. | 5.34 | 3.87 | 6.45 | 4.99 | 3.09 | 2.86 | 4.15 |
| Ba[††] | 102 | 40 | 540 | 391 | 79 | 34 | 28 | 233 | 44 | 108 | 68 | 2108 |
| Rb | 29 | 3 | 46 | 76 | 14 | 3 | 8 | 48 | 2 | 30 | 7 | 8 |
| Sr | 246 | 128 | 46 | 305 | 264 | 187 | 150 | 232 | 152 | 195 | 135 | 271 |
| Y | 60 | 27 | 151 | 50 | 36 | 30 | 42 | 37 | 25 | 43 | 40 | 32 |
| Zr | 273 | 121 | 509 | 126 | 161 | 141 | 201 | 197 | 108 | 197 | 177 | 79 |
| Nb | 36.00 | 14.78 | 88.06 | 8.20 | 19.00 | 13.55 | 22.27 | 22.47 | 11.28 | 23.00 | 19.34 | 4.29 |
| Th | 2.08 | 2.16 | 10.05 | N.D. | 1.30 | 1.48 | 1.61 | 1.64 | 0.85 | 3.00 | N.D. | 0.29 |
| Pb | N.D. | 4.32 | 5.29 | 2.00 | N.D. | 1.45 | 1.02 | 1.21 | N.D. | 2.00 | N.D. | 0.23 |
| Ga | N.D. | 25 | 25 | 20 | N.D. | 26 | 19 | 20 | 16 | 20 | 19 | 17 |
| Zn | 164 | 99 | 121 | 155 | 157 | 77 | 130 | 169 | 80 | 144 | 117 | 92 |
| Cu | 23 | 118 | 2 | 53 | 57 | 45 | 106 | 49 | 86 | 57 | 113 | 54 |
| Ni | 15 | 69 | 12 | 147 | 31 | 39 | 38 | 37 | 50 | 34 | 26 | 171 |
| V | 331 | 246 | 11 | 256 | 303 | 277 | 357 | 294 | 230 | 314 | 345 | 287 |
| Cr | 8 | 232 | 0 | 366 | 46 | 123 | 58 | 125 | 198 | 59 | 36 | 366 |
| Hf | 7 | N.D. | 17 | 3 | 5 | 3 | 5 | 5 | 3 | N.D. | N.D. | 2 |
| Cs | N.D. | N.D. | 0.07 | N.D. | N.D. | N.D. | N.D. | 1.89 | N.D. | N.D. | N.D. | 0.66 |
| Sc | 28.00 | 32.38 | 2.20 | 40.00 | 34.00 | 36.60 | 37.00 | 31.60 | 34.10 | 32.00 | 43.31 | 43.40 |
| Ta | 2.12 | N.D. | 6.03 | 0.49 | 1.12 | 0.91 | 1.56 | 1.56 | 0.78 | N.D. | N.D. | 0.29 |
| U | N.D. | N.D. | 1.84 | N.D. | N.D. | 0.28 | 0.43 | 0.44 | 0.25 | N.D. | N.D. | 0.10 |
| La | 20.20 | N.D. | 74.70 | 8.73 | 11.80 | 13.49 | 16.35 | 15.22 | 9.11 | 9.00 | 23.16 | 4.52 |
| Ce | 55.20 | 17.27 | 150.17 | 19.32 | 30.80 | 26.99 | 36.69 | 32.74 | 20.01 | 53.00 | 38.27 | 10.63 |
| Pr | N.D. | N.D. | 18.26 | 2.78 | N.D. | 3.38 | 4.84 | 4.35 | 2.65 | N.D. | N.D. | 1.56 |
| Nd | N.D. | N.D. | 77.60 | 15.06 | N.D. | 15.87 | 23.12 | 20.75 | 12.73 | N.D. | N.D. | 8.41 |
| Sm | 8.28 | N.D. | 20.98 | 4.46 | 5.00 | 4.52 | 7.08 | 6.34 | 3.95 | N.D. | N.D. | 2.99 |
| Eu | 3.04 | N.D. | 3.51 | 1.54 | 1.84 | 1.62 | 2.39 | 2.31 | 1.44 | N.D. | N.D. | 1.20 |
| Gd | N.D. | N.D. | 22.06 | 5.86 | N.D. | 5.17 | 7.97 | 7.25 | 4.61 | N.D. | N.D. | 4.17 |
| Tb | 1.23 | N.D. | 4.14 | 1.08 | N.D. | 0.90 | 1.36 | 1.20 | 0.79 | N.D. | N.D. | 0.79 |
| Dy | N.D. | N.D. | 26.34 | 7.49 | N.D. | 5.58 | 8.20 | 7.22 | 4.83 | N.D. | N.D. | 5.46 |
| Ho | N.D. | N.D. | 5.48 | 1.66 | N.D. | 1.13 | 1.63 | 1.42 | 0.98 | N.D. | N.D. | 1.20 |
| Er | N.D. | N.D. | 15.28 | 4.81 | N.D. | 3.01 | 4.16 | 3.53 | 2.48 | N.D. | N.D. | 3.36 |
| Tm | N.D. | N.D. | 2.25 | 0.70 | N.D. | 0.43 | 0.57 | 0.49 | 0.33 | N.D. | N.D. | 0.49 |
| Yb | 4.88 | N.D. | 13.99 | 4.22 | 2.98 | 2.63 | 3.43 | 2.84 | 2.03 | N.D. | N.D. | 3.16 |
| Lu | 0.77 | N.D. | 2.13 | 0.60 | 0.49 | 0.41 | 0.52 | 0.42 | 0.31 | N.D. | N.D. | 0.50 |

[†]Lat/Long in hddd°mm.mmm' based on NAD27 CONUS datum.
[‡]Magma type determined using immobile trace-element discrimination diagrams. WPB—within-plate basalt; WPG—within-plate granite; E-MORB—enriched mid-ocean-ridge basalt.
[§]$FeO^{T}$—total iron as FeO.
[#]Normalized to 100% loss on ignition (LOI) free.
[††]If all trace elements are reported, analysis of Y, Zr, Cr, V, and Ni was by X-ray fluorescence (XRF); others were by inductively coupled plasma–mass spectrometry (ICP-MS). Otherwise, all analysis was done by XRF.
[‡‡]N.D.—no data.
[§§]Sample from Metzger et al. (2002).

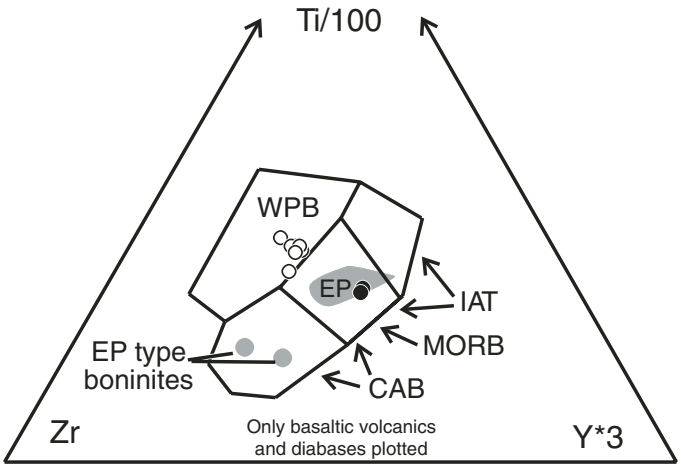


Figure 6. Ti-Zr-Y discrimination diagram (Pearce and Cann, 1973) for basalts from the Iron Mountain unit along with a shaded field and a labeled boninite for basalts of the Esmeralda Peaks (EP) unit. Symbols are the same as Figure 9. IAT—island-arc tholeiite; WPB—within-plate basalt; MORB—mid-ocean-ridge basalt; CAB—calc-alkaline basalt.

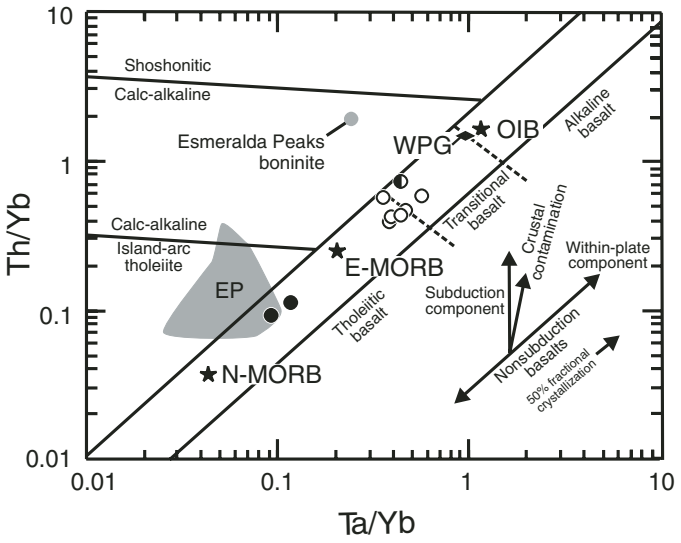


Figure 7. Th/Yb-Ta/Yb discrimination diagram (Pearce, 1982) for Iron Mountain basalts and rhyolite and a shaded field and a labeled boninite for volcanic rocks of the Esmeralda Peaks (EP) unit. Normal (N) MORB, enriched (E) MORB, and within-plate basalt (WPB) average values are from Sun and McDonough (1989). Within-plate granite (WPG) is from Pearce et al. (1984). Lau and Mariana back-arc basin fields were compiled by Harper (2003). Symbols are the same as Figure 9. OIB—ocean-island basalt.

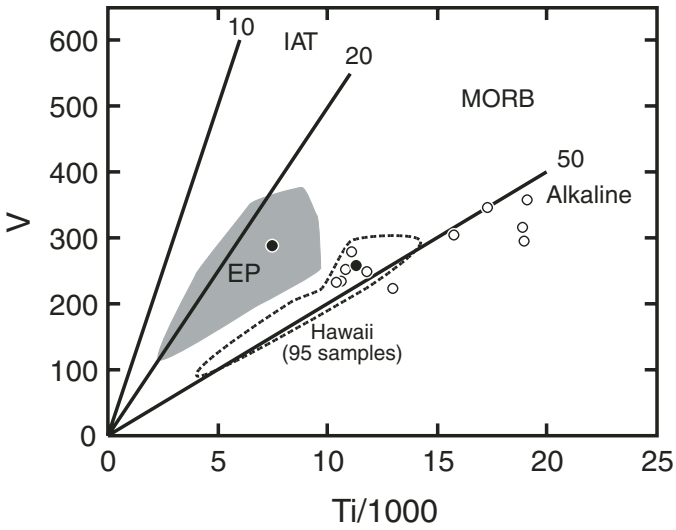


Figure 8. Ti-V discrimination diagram (Shervais, 1982) for Iron Mountain basalts along with a shaded field for basalts of the Esmeralda Peaks (EP) unit. Only mafic rocks are shown. Calc-alkaline basalts are excluded because Ti-V changes with fractionation. The Hawaii field was compiled from the GEOROC geochemical database (http://georoc.mpch-mainz.gwdg.de/georoc/). Symbols are the same as Figure 9. MORB—mid-ocean-ridge basalt.

## DISCUSSION

The newly defined Iron Mountain unit occurs along the southern margin of the Ingalls ophiolite complex. It is distinguished from other units in the complex by its Early Jurassic age (ca. 192 Ma; Fig. 10; Table 2), oolitic (Fig. 5) and pelagic limestone, within-plate magmatic affinities (Figs. 6, 7, 8, and 9), and rhyolite.

The Th/Yb-Ta/Yb and MORB-normalized diagrams (Figs. 7 and 9) are compatible with the rhyolite fractionating from the Iron Mountain basalt magma. Formation from partial melting of altered basalt, however, cannot be ruled out (Pearce, 1996b; Gunnarsson et al., 1998). "Granitic" magmas that have fractionated from within-plate basalt occur in small volume in ocean-island settings (e.g., within-plate granites on Ascension Island; Figs. 7 and 9) (Harris, 1983; Pearce, 1996b) and have been observed in other fossil seamounts (e.g., Snow Mountain volcanic complex; MacPherson, 1983).

The within-plate basalt affinities of these basalts suggest that the Iron Mountain unit formed as a seamount (Fig. 11A). The oolitic limestones (Fig. 5) and the disarticulation of fossil fragments within the limestone indicate deposition above wave base. Also, the highly vesicular nature of the Iron Mountain basalts is consistent with shallow-water eruption (Moore, 1970). The hemipelagic limestone and chert, however, imply deposition in deeper water during part of the formation of the Iron Mountain unit (Fig. 11B). Schmincke and Sumita (1998) and Schmidt and Schmincke (1999) indicated that seamounts are associated with locally derived sediments and explosive eruptions. The broken pillow breccia, basalt breccia, and hyaloclastite of the Iron Mountain unit probably represent these types of deposits.

For the Iron Mountain unit, we propose a seamount origin that formed within close proximity to a spreading ridge (Fig. 11A). This is based primarily on the transitional within-plate basalt to E-MORB geochemical affinities and tholeiitic,

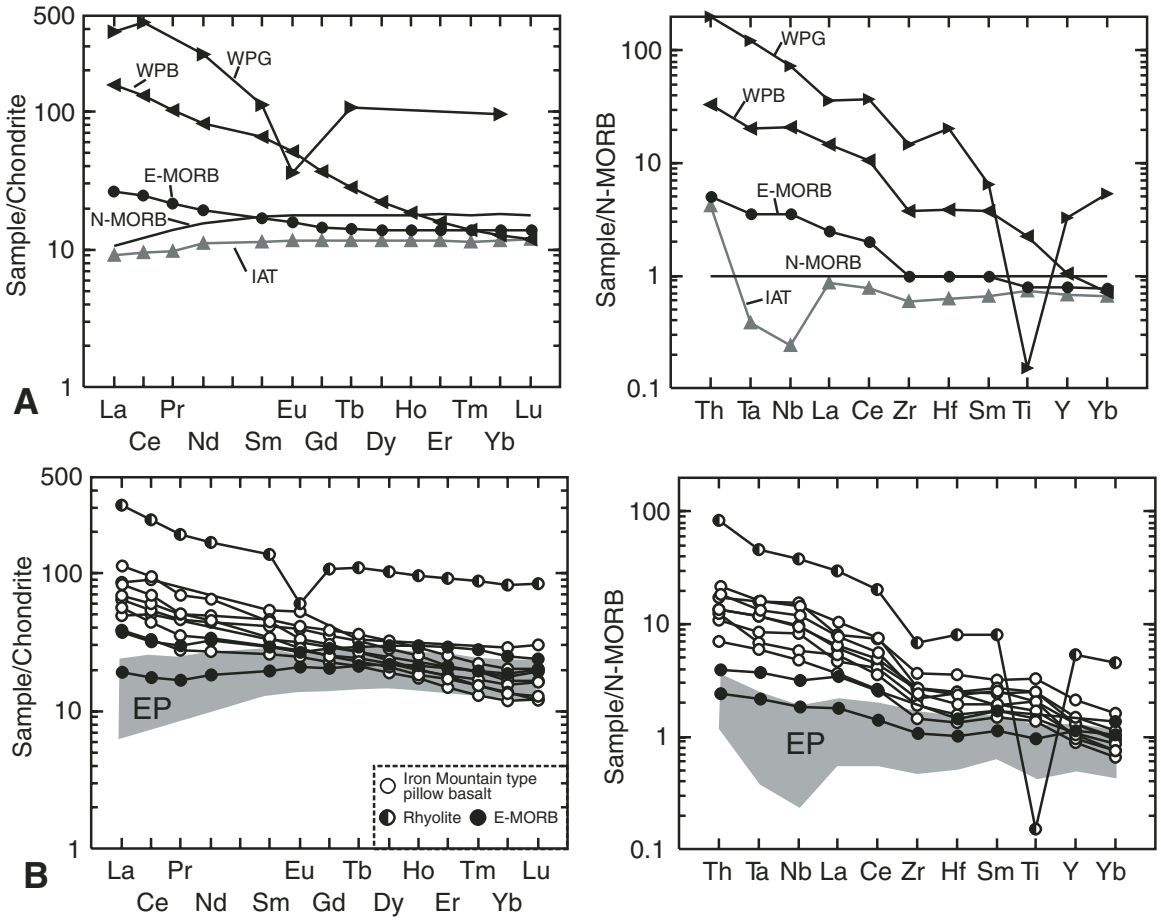


Figure 9. Chondrite- and mid-ocean-ridge basalt (MORB)–normalized diagrams. (A) Representative samples of different magma types including normal (N) MORB, enriched (E) MORB, within-plate basalt (WPB) (Sun and McDonough, 1989), island-arc tholeiite (IAT) (sample SSS5–4; Pearce et al., 1995), and within-plate granite (WPG) (Pearce et al., 1984). Chondrite- and MORB-normalizing values are from Sun and McDonough (1989). (B) Ten basalt samples and one rhyolite from the Iron Mountain unit along with a shaded field for Esmeralda Peaks (EP) samples (boninite not plotted).

rather than alkaline, compositions (Figs. 6, 7, 8, and 9). Transitional within-plate basalt to E-MORB compositions form where a mantle plume has interacted with an active spreading ridge (Shervais, 1982; Pearce, 1996a; Harpp and White, 2001). Also, Schmincke (2004) suggested that seamounts that form in close proximity to active mid-ocean spreading ridges are tholeiitic, whereas those formed in open-ocean basins are more alkaline. The minor graywacke associated with the sediments located on the Iron Mountain unit volcanics suggests that this seamount formed near a continent or arc.

The Th/Yb-Ta/Yb, chondrite-, and MORB-normalized diagrams (Figs. 7 and 9) imply that the Iron Mountain unit did not originate from a similar mantle to the ca. 161 Ma Esmeralda Peaks unit. The εNd(t) data for these two units, +6 to +7 for the Iron Mountain unit and +8 to +9 for the Esmeralda Peaks unit, also support this interpretation (MacDonald et al., 2002).

The Early Jurassic age of the Iron Mountain unit and Late Jurassic age of the Esmeralda Peaks unit suggest that the Ingalls ophiolite complex is polygenetic. A possible polygenetic origin for the Ingalls complex was previously proposed by Tabor et al. (1982) and Miller et al. (1993). The Iron Mountain unit most likely represents rifted basement of the Esmeralda Peaks unit (Fig. 11C), at least along the southern margin of the complex where Esmeralda Peaks basalts overlie the Iron Mountain unit at Sheep Mountain (Fig. 4). The Esmeralda Peaks unit north of the Iron Mountain outcrop belt may have formed by Late Jurassic seafloor spreading and associated transform faulting, which apparently affected portions of the ophiolite complex (Fig. 11C). All crustal units within the complex were structurally mixed together during mélange formation (Fig. 11D).

A modern-day analog for a rift-edge facies is the western portion of the Lau back-arc basin (Hawkins, 1995, 2003). In this part of the basin, older crust is rifted apart by younger propagating spreading ridges and covered by basalt flows (Hawkins, 1995, 2003, and references within). We suggest that the Iron Mountain unit is analogous to the rifted older basement

TABLE 2. U-Pb DATA FOR SAMPLE BL-150 (RHYOLITE OF IRON MOUNTAIN UNIT)

| Fractions | Weight (mg) | Conc. U | Ages (Ma) | | | | | | | | | | | | Total common Pb (pg) |
|---|---|---|---|---|---|---|---|---|---|---|---|---|---|---|---|
| | | | Pb† (ppm) | $^{206}Pb/^{204}Pb$‡ | $^{206}Pb/^{238}U$§ | Error (%) | $^{207}Pb/^{235}U$§ | Error (%) | $^{207}Pb/^{206}Pb$ | Error (%) | $^{206}Pb/^{238}U$ | $^{207}Pb/^{235}U$ | $^{207}Pb/^{206}Pb$ | Corr. coeff. | |
| SquatPrism1(1) | 0.0004 | 950.1 | 31.3 | 506.49 | 0.03021 | –0.47 | 0.20811 | –1.4 | 0.04996 | –1.2 | 191.9 | 192 | 193 | 0.47 | 1.5 |
| SquatPrism2(1) | 0.0004 | 1396 | 45.9 | 1002.1 | 0.03026 | –0.23 | 0.20937 | –0.59 | 0.05018 | –0.53 | 192.2 | 193 | 203.3 | 0.46 | 1.1 |
| MediumPrisms1 | 0.0008 | 838.1 | 27.8 | 616.58 | 0.03029 | –0.32 | 0.2087 | –0.58 | 0.04997 | –0.45 | 192.4 | 192.5 | 193.6 | 0.62 | 2.2 |
| MediumPrisms2 | 0.0007 | 644.9 | 21.7 | 611.5 | 0.03021 | –0.34 | 0.20848 | –0.51 | 0.05004 | –0.37 | 191.9 | 192.3 | 197.1 | 0.7 | 1.5 |
| MediumPrisms3 | 0.0007 | 564.7 | 18.9 | 500.72 | 0.03016 | –0.42 | 0.20831 | –0.54 | 0.05008 | –0.33 | 191.6 | 192.1 | 198.7 | 0.8 | 1.6 |

†Radiogenic Pb.
‡Measured ratio corrected for fractionation only. All Pb isotope ratios were measured using single-collector Daly mode and were corrected for fractionation using 0.18%/amu.
§Corrected for fractionation, spike, and initial common Pb. After subtraction of blank Pb (<5 pg), common Pb corrections were unnecessary.

of the Lau basin, and the Esmeralda Peaks unit is similar to the younger rift-related flows or oceanic crust created by seafloor spreading after rifting.

An alternative hypothesis is that the Iron Mountain unit is a transform-edge facies (Fig. 11C). In this scenario, the unit represents older basement juxtaposed against the Esmeralda Peaks unit and mantle peridotite across the Navaho Divide fault zone (Fig. 11C), which Miller (1985) interpreted as a fossil fracture zone. The Esmeralda Peaks basalts that overlie the Iron Mountain unit at Sheep Mountain (Figs. 3 and 4) may thus represent flows across the fracture zone.

Seamounts also occur as tectonic "slices" within fossil subduction zones (MacPherson, 1983; Dewey, 2003). The Navaho Divide fault zone mélange could have formed in a subduction rather then a fracture-zone setting; however, this fault zone lacks the high-pressure–low-temperature metamorphism that is associated with subduction zones (Ernst, 1973). In addition, Miller and Mogk (1987) and MacDonald et al. (2005, this volume, chapter 4) outlined data that support a fracture-zone origin for the Navaho Divide fault zone.

This setting of younger ophiolitic rocks built upon older ophiolitic rocks is similar to that inferred for the Devils Elbow and Preston Peak "rift-edge facies" of the Josephine ophiolite, in the Klamath Mountains of northwest California and southwest Oregon (Fig. 1) (Saleeby et al., 1982; Wyld and Wright, 1988). These rift-edge facies, and a similar facies recently recognized along the northern margin of the Josephine ophiolite, were built upon the Rattlesnake Creek terrane and its correlative units (Fig. 1) (Saleeby et al., 1982; Wyld and Wright, 1988; Yule et al., 2006). The Rattlesnake Creek terrane is similar to the Iron Mountain unit in its fossil ages, presence of sparse limestone, and within-plate basalt to MORB geochemical affinities (Wright and Wyld, 1994; Giaramita and Harper, 2006; Yule et al., 2006). The Josephine ophiolite, including the Devils Elbow remnant, and the Esmeralda Peaks unit of the Ingalls ophiolite complex have similar ages and IAT-MORB geochemical affinities (Wright and Wyld, 1986; Wyld and Wright, 1988; Metzger et al., 2002; Harper, 2003; MacDonald et al., this volume, chapter 4). The sedimentary rocks that sit on the Esmeralda Peaks unit and Josephine ophiolite have been correlated based on radiolarian ages of cherts and age of detrital zircon in sandstones (Miller et al., 2003). These relationships suggest

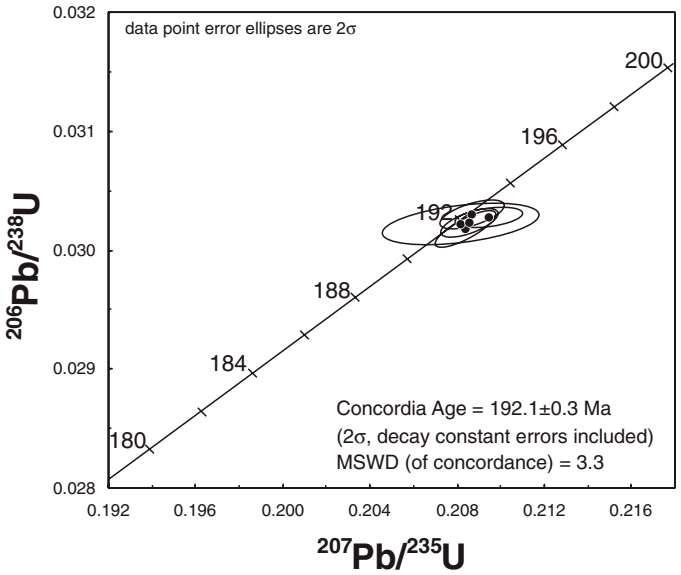


Figure 10. Concordia diagram for a rhyolite (sample BL-150) from the Iron Mountain unit (see Table 3). Ellipses reflect 2σ error. MSWD—mean square of weighted deviates.

a similar origin for the Ingalls ophiolite complex and the Josephine ophiolite and its rift-edge facies (Fig. 1).

It should be noted that the lithologies, geochemical affinities, and fossil ages of the Rattlesnake Creek terrane are more diverse than the Iron Mountain unit (Wright and Wyld, 1994; Yule et al., 2006). Also, the Rattlesnake Creek terrane consists of a mélange basement and volcanic cover sequence (Wright and Wyld, 1994), which is not seen in the Iron Mountain unit. Therefore, the Iron Mountain unit is not a perfect correlation to the Rattlesnake Creek terrane.

## CONCLUSION

The Iron Mountain unit: (1) is a newly recognized component of the Ingalls ophiolite complex; (2) is Early Jurassic in age; (3) consists of vesicular basalt, broken pillow breccia, mudstone, lesser limestone, and minor rhyolite, hyaloclastite, chert, tuff, and sandstone; (4) was formed as an off-axis seamount (Fig. 11A),

TABLE 3. EARLY JURASSIC RADIOLARIAN AGES FROM THE INGALLS OPHIOLITE COMPLEX

| Sample no. | Locality | Latitude (°N) | Longitude (°W) | Age | Radiolaria |
|---|---|---|---|---|---|
| BL-21-1† | Sheep Mtn. | 47°24′12.5″ | 120°38′53.2″ | Early Jurassic (Pliensbachian undifferentiated) | *Canoptum* sp. ?, *Noritus* sp., *Praeconocaryomma* sp., *Zartus mostleri*§ |
| BL-22-1† | Sheep Mtn. | 47°24′10.0″ | 120°38′55.2″ | Probably Early Jurassic (Pliensbachian ?) | *Canoptum* sp. ?, *Praeconocaryomma* sp., *Praeconocaryomma immodica*§ |
| BL-48-1† | Eastern flank of Iron Mtn. | 47°24′27.5″ | 120°41′00.0″ | Early Jurassic (probably late Pliensbachian) | *Canoptum* sp. Aff. *C. rugosum*#, *Canutus haimaensis*††, *Canutus izeensis*††, *Hsuum mulleri*††, *Praeconocaryomma parvimamma*#, *Protopsium* sp.#, *Trillus elkhornensis*§, *Zartus* sp. Aff. *Z. mostleri*§ |
| IM-74E‡ | West side of Negro Creek | 47° 25′ 03.0″ | 120° 44′ 34.5″ | Upper Pliensbachian to Middle Toarcian | *Paracanoptum annulatum*#, *Parahsuum* sp. |

†Fossil and age determinations made by Blome (1992).
‡Fossil and age determinations made by Pessagno (2004).
§Pessagno and Blome (1980).
#Pessagno and Poisson (1979).
††Pessagno and Whalen (1982).

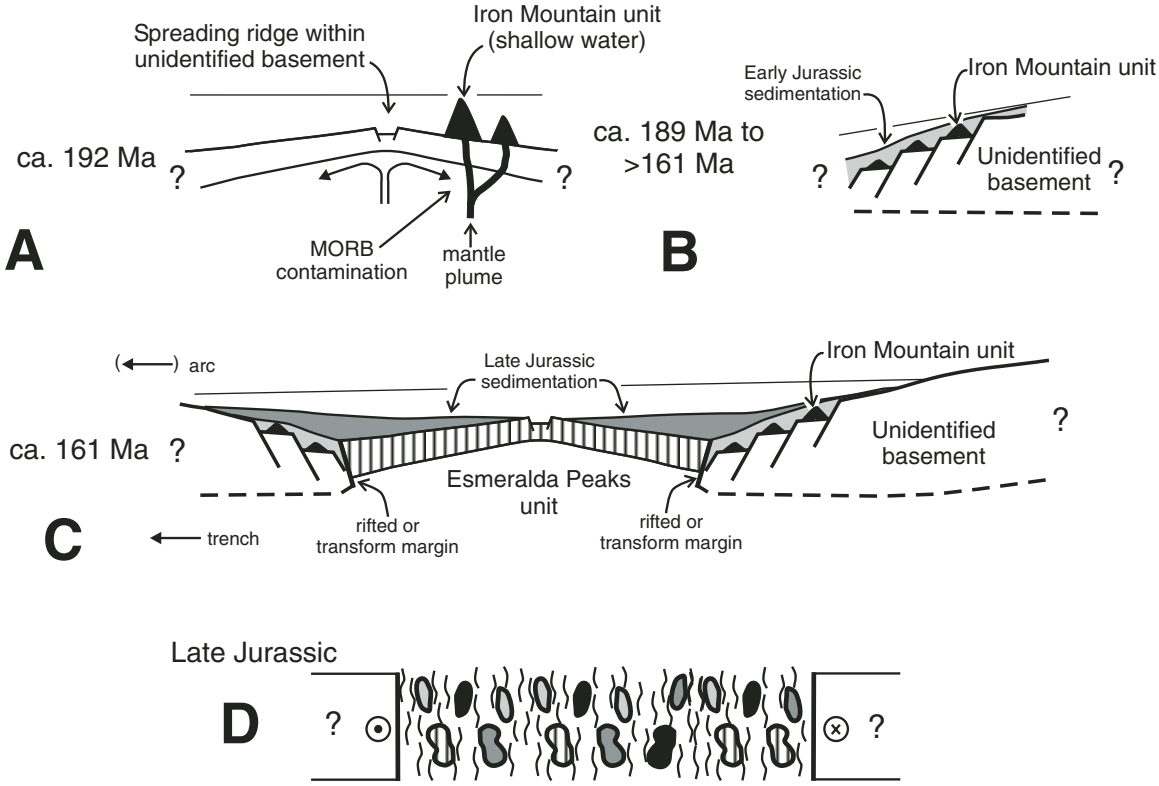


Figure 11. Tectonic diagram for the Ingalls ophiolite complex. (A) Initial formation of the Iron Mountain unit as a seamount during the Early Jurassic. (B) Deposition of the Early Jurassic sediments. (C) Formation of the Esmeralda Peaks unit during the Late Jurassic by possible rifting of the older Iron Mountain unit. (D) Mélange formation that enclosed most units.

with clastic and pelagic sedimentation occurring later (Fig. 11B); (5) was rifted apart during the Late Jurassic, forming the basement to the Esmeralda Peaks unit (Fig. 11C); and (6) was then structurally mixed with other crustal units of the Ingalls ophiolite complex in the mélange of the Navaho Divide fault zone (Fig. 11D). The identification of the Iron Mountain unit indicates that the Ingalls ophiolite complex is polygenetic.

## ACKNOWLEDGMENTS

This research was supported by National Science Foundation (NSF) grant EAR-0003444 to G.D. Harper and NSF grant EAR-0087829 to R.B. Miller and J.S. Miller. J.H. MacDonald was funded by GSA Research Grant 6951-01, a Sigma Xi Grant-in-Aid of Research, and the Department of Earth and

Atmospheric Science, State university of New York (SUNY) at Albany. E. Pessagno did outstanding work in identifying radiolarians. Marty Giaramita and John Shervais provided us with thoughtful and critical reviews that greatly improved this paper. We would like to thank Jeff Karson, Nancy Riggs, and Bill Kidd for reviewing early drafts of this paper. John Shervais and Jim Wright proved to be first-class editors of this volume. J. Arnason, B. Fletcher, and K. Hollocher assisted greatly with inductively coupled plasma–mass spectrometry (ICP-MS) analysis at Union College. We thank Scott McPeek, Mike Siudy, Ron Karpowicz, and Cindy Schultz for assistance in the field, Dan Redell for assistance with sample preparation, and the 2003 GSA National Meeting Ingalls Ophiolite field trip participants for their insightful discussions. Finally, we acknowledge Cliff Hopson for his early recognition of the significance of Jurassic ophiolitic and arc rocks in the Washington Cascades and thank him for his enthusiasm and encouragement of our research over the past 30 yr.

## REFERENCES CITED

Anonymous, 1972, Penrose Field Conference: Ophiolites: Geotimes, v. 17, p. 24–25.

Dewey, J., 2003, Ophiolites and lost oceans: Rifts, ridges, arcs, and/or scrapings, *in* Dilek, Y., and Newcomb, S., eds., Ophiolite Concept and the Evolution of Geological Thought: Geological Society of America Special Paper 373, p. 153–158.

De Wit, M.J., and Stern, C.R., 1981, Variations in the degree of crustal extension during formation of a back-arc basin: Tectonophysics, v. 72, p. 229–260, doi: 10.1016/0040-1951(81)90240-7.

Dilek, Y., 2003, Ophiolite concept and its evolution, *in* Dilek, Y., and Newcomb, S., eds., Ophiolite Concept and the Evolution of Geological Thought: Geological Society of America Special Paper 373, p. 1–16.

Eddy, C.A., Dilek, Y., Hurst, S., and Moores, E.M., 1998, Seamount formation and associated caldera complex and hydrothermal mineralization in ancient oceanic crust, Troodos ophiolite (Cyprus): Tectonophysics, v. 292, p. 189–210, doi: 10.1016/S0040-1951(98)00064-X.

Ernst, W.G., 1973, Blueschist metamorphism and *P-T* regimes in active subduction zones, Experimental petrology and global tectonics: Tectonophysics, v. 17, p. 255–272, doi: 10.1016/0040-1951(73)90006-1.

Giaramita, M.J., and Harper, G.D., 2006, Geochemistry of ophiolitic rocks associated with the western part of the Elk outlier of the western Klamath terrane, southwestern Oregon, *in* Snoke, A.W., and Barnes, C.G., eds., Geological Studies in the Klamath Mountains Province, California and Oregon: Geological Society of America Special Paper 410, p. 153–176.

Gradstein, F.M., Ogg, J.G., and Smith, A.G., eds., 2004, A Geologic Time Scale 2004: Cambridge, England, Cambridge University Press, 384 p.

Gray, J.E., 1982, Petrology and Geochemistry of the Eastern Portion of the Ingalls Complex, Central Washington Cascades [M.S. thesis]: Lawrence, Kansas, University of Kansas, 63 p.

Gunnarsson, B., Marsh, B.D., and Taylor, H.P., Jr., 1998, Generation of Icelandic rhyolites; silicic lavas from the Torfajokull central volcano: Journal of Volcanology and Geothermal Research, v. 83, p. 1–45, doi: 10.1016/S0377-0273(98)00017-1.

Harper, G.D., 2003, Tectonic implications of boninite, arc tholeiite, and MORB magma types in the Josephine ophiolite, California-Oregon, *in* Dilek, Y., and Robinson, P.T., eds., Ophiolites in Earth History: Geological Society [London] Special Publication 218, p. 207–229.

Harper, G.D., Saleeby, J.B., and Heizler, M., 1994, Formation and emplacement of the Josephine ophiolite and the Nevadan orogeny in the Klamath Mountains, California-Oregon; U-Pb zircon and $^{40}Ar/^{39}Ar$ geochronology: Journal of Geophysical Research, v. 99, no. B3, p. 4293–4321, doi: 10.1029/93JB02061.

Harper, G.D., Miller, R.B., MacDonald, J.H., Jr., Miller, J.S., and Mlinarevic, A.N., 2003, Evolution of a polygenetic ophiolite: The Jurassic Ingalls ophiolite, Washington Cascades, *in* Swanson, T.W., ed., Western Cordillera and Adjacent Areas: Boulder, Colorado, Geological Society of America Field Guide 4, p. 251–265.

Harpp, K.S., and White, W.M., 2001, Tracing a mantle plume: Isotopic and trace element variations of Galapagos seamounts: Geochemistry, Geophysics, Geosystems, v. 2, doi: 10.1029/2000GC000137.

Harris, C., 1983, The petrology of lavas and associated plutonic inclusions of Ascension Island: Journal of Petrology, v. 24, p. 424–470.

Hawkins, J.W., 1995, Evolution of the Lau Basin; insights from ODP Leg 135, *in* Taylor, B., and Natland, J., eds., Active Margins and Marginal Basins of the Western Pacific: American Geophysical Union Geophysical Monograph 88, p. 125–173.

Hawkins, J.W., 2003, Geology of supra-subduction zones—Implications for the origin of ophiolites, *in* Dilek, Y., and Newcomb, S., eds., Ophiolite Concept and the Evolution of Geological Thought: Geological Society of America Special Paper 373, p. 227–268.

Hopson, C.A., Mattinson, J.M., and Pessagno, E.A., Jr., 1981, Coast Range ophiolite, western California, *in* Ernst, W.G., ed., The Geotectonic Development of California: Rubey Volume I: Prentice-Hall, Englewood Cliffs, New Jersey, p. 418–510.

Ludwig, K.R., 1989, PbDat for MSDOS: A Computer Program for IBM-PC Compatibles for Processing Raw Pb-U-Th Data, Version 1.06: U.S. Geological Survey Open-File Report 88-542, 40 p.

Ludwig, K.R., 1990, ISOPLOT: A Plotting and Regression Program for Radiogenic Pb Isotope Data, for IBM-PC Compatible Computers, Version 2.02: U.S. Geological Survey Open-File Report 88-557, 44 p.

MacDonald, J.H., Jr., Harper, G.D., Miller, R.B., and Miller, J.S., 2002, Within-plate magmatic affinities of a lower pillow unit in the Ingalls ophiolite complex, northwest Cascades, Washington: Geological Society of America Abstracts with Programs, v. 34, no. 5, p. 22.

MacDonald, J.H., Jr., Mlinarevic, A., Harper, G.D., Miller, R.B., Miller, J.S., and Schultz, C.E., 2005, Sedimentary serpentinites of the Ingalls ophiolite complex: Further evidence of a fracture zone setting: Geological Society of America Abstracts with Programs, v. 37, no. 4, p. 86.

MacDonald, J.H., Jr., Harper, G.D., Miller, R.B., Miller, J.S., Mlinarevic, A., and Schultz, C.E., 2008, this volume, The Ingalls ophiolite complex, central Cascades, Washington: Geochemistry, tectonic setting, and regional correlations, *in* Wright, J.E., and Shervais, J.W., eds., Ophiolites, Arcs, and Batholiths: A Tribute to Cliff Hopson: Geological Society of America Special Paper 438, doi: 10.1130/2008.2438(04).

MacPherson, G.J., 1983, The Snow Mountain volcanic complex; an on-land seamount in the Franciscan terrane, California: The Journal of Geology, v. 91, p. 73–92.

Matzel, J.P., Bowring, S.A., and Miller, R.B., 2006, Time scales of pluton construction at differing crustal levels: Examples from the Mount Stuart and Tenpeak intrusions, north Cascades, Washington: Geological Society of America Bulletin, v. 118, p. 1412–1430, doi: 10.1130/B25923.1.

Metzger, E.P., Miller, R.B., and Harper, G.D., 2002, Geochemistry and tectonic setting of the ophiolitic Ingalls complex, north Cascades, Washington; implications for correlations of Jurassic Cordilleran ophiolites: The Journal of Geology, v. 110, p. 543–560, doi: 10.1086/341759.

Meyer, J., Mercolli, I., and Immenhauser, A., 1996, Off-ridge alkaline magmatism and seamount volcanoes in the Masirah Island ophiolite, Oman: Tectonophysics, v. 267, p. 187–208, doi: 10.1016/S0040-1951(96)00094-7.

Miller, J.S., Miller, R.B., Wooden, J.L., and Harper, G.D., 2003, Geochronologic links between the Ingalls ophiolite, north Cascades, Washington, and the Josephine ophiolite, Klamath Mts., Oregon and California: Geological Society of America Abstracts with Programs, v. 35, no. 6, p. 113.

Miller, R.B., 1980, Structure, Petrology and Emplacement of the Ingalls Complex, North-Central Cascade Mountains, Washington [Ph.D. thesis]: Seattle, Washington, University of Washington, 422 p.

Miller, R.B., 1985, The ophiolitic Ingalls Complex, north-central Cascade Mountains, Washington: Geological Society of America Bulletin, v. 96, p. 27–42, doi: 10.1130/0016-7606(1985)96<27:TOICNC>2.0.CO;2.

Miller, R.B., and Mogk, D.W., 1987, Ultramafic rocks of a fracture-zone ophiolite, north Cascades, Washington: Tectonophysics, v. 142, p. 261–289, doi: 10.1016/0040-1951(87)90127-2.

Miller, R.B., Mattinson, J.M., Goetsch Funk, S.A., Hopson, C.A., and Treat, C.L., 1993, Tectonic evolution of Mesozoic rocks in the southern and central Washington Cascades, *in* Dunne, G.C., and McDougall, K.A., eds., Mesozoic Paleogeography of the Western United States: Pacific Section, Society of Economic Paleontologists and Mineralogists, Field Trip Guidebook, part II, v. 71, p. 81–98.

Mlinarevic, A.N., Miller, R.B., Harper, G.D., MacDonald, J.H., Jr., and Miller, J.S., 2003, Nodal basin (?) sedimentation in an ancient oceanic fracture zone, Ingalls ophiolite complex, Washington: Geological Society of America Abstracts with Programs, v. 35, no. 6, p. 513.

Moore, J.G., 1970, Water content of basalts erupted on the ocean floor: Contributions to Mineralogy and Petrology, v. 28, p. 272–279, doi: 10.1007/BF00388949.

Moores, E.M., 1982, Origin and emplacement of ophiolites: Reviews of Geophysics and Space Physics, v. 20, p. 735–760.

Palfy, J., Smith, P. L., and Mortensen, J.K., 2000, A U-Pb and $^{40}Ar/^{39}Ar$ time scale for the Jurassic: Canadian Journal of Earth Sciences, v. 37, no. 6, p. 923-944.

Pearce, J.A., 1982, Trace element characteristics of lavas from destructive plate boundaries, *in* Thorpe, R.S., ed., Andesites: Orogenic Andesites and Related Rocks: New York, John Wiley and Sons, p. 525–548.

Pearce, J.A., 1996a, A user's guide to basalt discrimination diagrams, *in* Wyman, D.A., ed., Trace Element Geochemistry of Volcanic Rocks; Applications for Massive Sulphide Exploration: Geological Association of Canada, Short Course Notes, v. 12, p. 79–113.

Pearce, J.A., 1996b, Source and setting of granitic rocks: Episodes, v. 19, p. 120–125.

Pearce, J.A., and Cann, J.R., 1973, Tectonic setting of basic volcanic rocks determined using trace element analyses: Earth and Planetary Science Letters, v. 19, p. 290–300, doi: 10.1016/0012-821X(73)90129-5.

Pearce, J.A., Harris, N.B.W., and Tindle, A.G., 1984, Trace element discrimination diagrams for the tectonic interpretation of granitic rocks: Journal of Petrology, v. 25, p. 956–983.

Pearce, J.A., Baker, P.E., Harvey, P.K., and Luff, I.W., 1995, Geochemical evidence for subduction fluxes, mantle melting and fractional crystallization beneath the South Sandwich island arc: Journal of Petrology, v. 36, p. 1073–1109.

Pessagno, E.A., Jr., and Blome, C.D., 1980, Upper Triassic and Jurassic Pantanelliinae from California, Oregon, and British Columbia: Micropaleontology, v. 26, p. 225–273, doi: 10.2307/1485314.

Pessagno, E.A., Jr., and Poisson, A., 1979, Lower Jurassic Radiolaria from the Gumuslu allochthon of southwestern Turkey (Taurides Occidentales): Bulletin of the Mineral Research and Exploration Institute of Turkey, v. 92, p. 47–69.

Pessagno, E.A., Jr., and Whalen, P.A., 1982, Lower and Middle Jurassic Radiolaria (multicyrtid Nassellariina) from California, east-central Oregon and the Queen Charlotte Islands, B.C.: Micropaleontology, v. 28, p. 111–169, doi: 10.2307/1485228.

Saleeby, J.B., 1978, Kings River ophiolite, southwest Sierra Nevada foothills, California: Geological Society of America Bulletin, v. 89, p. 617–636, doi: 10.1130/0016-7606(1978)89<617:KROSSN>2.0.CO;2.

Saleeby, J.B., 1992, Petrotectonic and paleogeographic settings of the U.S. Cordilleran ophiolites, *in* Burchfiel, B.C., et al., eds., The Cordilleran Orogen: Conterminous U.S.: Boulder, Colorado, Geological Society of America, Geology of North America, v. G-3, p. 653–683.

Saleeby, J.B., and Sharp, W., 1980, Chronology of the structural and petrologic development of the southwest Sierra Nevada foothills, California: Geological Society of America Bulletin, v. 91, p. 317–320, 1416–1535.

Saleeby, J.B., Harper, G.D., Snoke, A.W., and Sharp, W.D., 1982, Time relations and structural-stratigraphic patterns in ophiolite accretion, west-central Klamath Mountains, California: Journal of Geophysical Research, ser. B, v. 87, p. 3831–3848.

Schmidt, R., and Schmincke, H.-U., 1999, Seamounts and island building, *in* Sigurdsson, H., et al., eds., Encyclopedia of Volcanoes: San Diego, Academic Press, p. 383–406.

Schmincke, H.-U., 2004, Volcanism: Berlin, Springer, 324 p.

Schmincke, H.-U., and Sumita, M., 1998, Volcanic evolution of Gran Canaria reconstructed from apron sediments; synthesis of Vicap Project Drilling, *in* Weaver, P.P.E., et al., Proceedings of the Ocean Drilling Program, Scientific Results, Volume 157: College Station, Texas, Ocean Drilling Program, p. 443–469.

Shervais, J.W., 1982, Ti-V plots and the petrogenesis of modern and ophiolitic lavas: Earth and Planetary Science Letters, v. 59, p. 101–118, doi: 10.1016/0012-821X(82)90120-0.

Shervais, J.W., Murchey, B., Kimbrough, D.L., Hanan, B.B., Renne, P.R., Snow, C.A., Schuman, M.Z., and Beaman, J., 2004, Multi-stage origin of the Coast Range ophiolite, California: Implications for the life cycle of supra-subduction zone ophiolites: International Geology Review, v. 46, p. 289–315.

Shervais, J.W., Schuman, M.M.Z., and Hanan, B.B., 2005, The Stonyford volcanic complex: a forearc seamount in the northern California Coast Ranges: Journal of Petrology, v. 46, p. 2091–2128, doi: 10.1093/petrology/egi048.

Smith, G.O., 1904, Description of the Mount Stuart Quadrangle: U.S. Geological Survey Atlas, Mount Stuart folio, no. 106, 10 p.

Southwick, D.L., 1962, Mafic and Ultramafic Rocks of the Ingalls-Peshastin Area, Washington, and Their Geologic Setting [Ph.D. thesis]: Baltimore, Maryland, Johns Hopkins University, 287 p.

Southwick, D.L., 1974, Geology of the Alpine-type ultramafic complex near Mount Stuart, Washington: Geological Society of America Bulletin, v. 85, p. 391–402, doi: 10.1130/0016-7606(1974)85<391:GOTAUC>2.0.CO;2.

Steiger, R.H., and Jäger, E., 1977, Subcommission on geochronology: Convention on the use of decay constants in geo- and cosmochronology: Earth and Planetary Science Letters, v. 36, p. 359–362, doi: 10.1016/0012-821X(77)90060-7.

Stern, C.R., and De Wit, M.J., 2003, Rocas Verdes ophiolite, southernmost South America: Remnants of progressive stages of development of oceanic-type crust in a continental margin back-arc basin, *in* Dilek, Y., and Robinson, P.T., eds., Ophiolites in Earth History: Geological Society [London] Special Publication 218, p. 665–683.

Sun, S.S., and McDonough, W.F., 1989, Chemical and isotopic systematics of oceanic basalts; implications for mantle composition and processes, *in* Saunders, A.D., and Norry, M.J., eds., Magmatism in the Ocean Basins: Geological Society [London] Special Publication 42, p. 313–345.

Tabor, R.W., Waitt, R.B., Jr., Frizzell, V.A., Jr., Swanson, D.A., Byerly, G.R., and Bentley, R.D., 1982, Geologic Map of the Wenatchee 1:100,000 Quadrangle, Central Washington: U.S. Geological Survey Miscellaneous Investigations Series I-1311, 26 p.

Tabor, R.W., Frizzell, V.A., Jr., Whetten, J.T., Waitt, R.B., Jr., Swanson, D.A., Byerly, G.R., Booth, D.B., Hetherington, M.J., and Zartman, R.E., 1987, Geologic Map of the Chelan 30′ by 60′ Quadrangle, Washington: U.S. Geological Survey Miscellaneous Investigations Series I-1661, 33 p.

Tabor, R.W., Frizzell, V.A., Jr., Booth, D.B., Waitt, R.B., Whetten, J.T., and Zartman, R.E., 1993, Geologic Map of the Skykomish River 30′ by 60′ Quadrangle, Washington: U.S. Geological Survey Miscellaneous Investigations Series I-1963, 42 p.

Tabor, R.W., Frizzell, V.A., Jr., Booth, D.B., and Waitt, R.B., 2000, Geologic Map of the Snoqualmie Pass 30′ by 60′ Quadrangle, Washington: U.S. Geological Survey Geologic Investigations Series I-2538, 57 p.

Wright, J.E., and Wyld, S.J., 1986, Significance of xenocrystic Precambrian zircon contained within the southern continuation of the Josephine ophiolite, Devils Elbow ophiolite remnant, Klamath Mountains, northern California: Geology, v. 14, no. 8, p. 671–674, doi: 10.1130/0091-7613(1986)14<671:SOXPZC>2.0.CO;2.

Wright, J.E., and Wyld, S.J., 1994, The Rattlesnake Creek terrane, Klamath Mountains, California: An early Mesozoic volcanic arc and its basement of tectonically disrupted oceanic crust: Geological Society of America Bulletin, v. 106, p. 1033–1056, doi: 10.1130/0016-7606(1994)106<1033:TRCTKM>2.3.CO;2.

Wyld, S.J., and Wright, J.E., 1988, The Devils Elbow ophiolite remnant and overlying Galice Formation: New constraints on the Middle to Late Jurassic evolution of the Klamath Mountains, California: Geological Society of America Bulletin, v. 100, p. 29–44, doi: 10.1130/0016-7606(1988)100<0029:TDEORA>2.3.CO;2.

Yule, J.D., Saleeby, J.B., and Barnes, C.G., 2006, A rift-edge facies of the Late Jurassic Rogue-Chetco arc and Josephine ophiolite, Klamath Mountains, Oregon, *in* Snoke, A.W., and Barnes, C.G., eds., Geological Studies in the Klamath Mountains Province, California and Oregon: Geological Society of America Special Paper 410, p. 53–76.

Manuscript Accepted by the Society 16 July 2007